ACS Energy LETTERS

http://pubs.acs.org/journal/aelccp

Moss-like Growth of Metal Electrodes: On the Role of Competing Faradaic Reactions and Fast Charging

J. X. Kent Zheng, Jiefu Yin, Tian Tang, and Lynden A. Archer*

Cite This: *ACS Energy Lett.* 2023, 8, 2113–2121

Read Online

ACCESS | Metrics & More | Article Recommendations | Supporting Information

ABSTRACT: Uncontrolled crystal growth during electroreduction of reactive metals in liquid electrolytes produces mossy metal deposits. Here, we use electroanalytical rotating disk electrode (RDE) studies to elucidate the origin of moss-like electrodeposition of metals. Competing Faradaic reactions on the electrode surface are shown to be the source of the phenomenon. A moss-like growth regime can be accessed by subtle shifts in electrolyte chemistry and deposition rate. For Zn—a metal that conventionally is not known to form moss-like electrodeposits—obvious moss-like patterns emerge at low-current densities in strongly alkaline electrolytes. Conversely, under conditions where the electroreduction rate is large relative to competing Faradaic reactions, moss-like Zn growth is eliminated. The same principle holds for Li metal deposition. On that basis, an empirical rule is proposed—an applied current density i that satisfies the relation $10\ i_s < i < 0.8\ i_{lim}$ is required for achieving favorable metal electrodeposit morphology and fast charging in batteries.

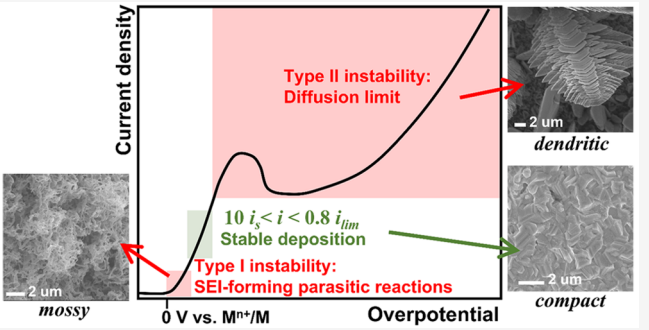

The "*dendritic*" growth of metal electrodeposits at planar substrates is now a well-known failure mode for secondary batteries and in electroplating processes. The term *dendritic* deposition has also been used in contemporary literature to loosely refer to a variety of fundamentally different electrodeposition processes that produce metal deposits with preferred growth parallel to the substrate normal vector and typically produces electrodeposits with porous, mossy morphologies.[1,2] Dendrites by etymology are tree-like, fractal structures that are actually the norm for crystal growth in systems driven far from equilibrium by external fields. For example, tree-like growth of a solid phase characterized by self-similarity is unambiguously understood in a large number of classical contexts to arise from transport limitations or symmetry, *e.g.*, alloy casting,[3] ice forming,[4] and traditional electroplating.[5] A large body of theoretical and experimental work has shown that electroplating of metals at high current densities, e.g., at current densities above the diffusion limit, produces classical dendritic deposits of metals such as Zn,[9] Mg,[2,3] and Cu.[6] On this basis, one would expect the dendritic growth to be eliminated at low current densities below the diffusion limit. This hypothesis has been tested extensively for Li metal deposition in battery anodes from a variety of perspectives, and the results are at best confusing—Li metal consistently deposits into porous, nonplanar structures composed of tortuous nano/microwires even at a very small current density and across vastly different electrolyte chemistries.[7] More detailed microscopy studies reveal that the porous, nonplanar structures do not follow a tree-like growth mode, in contrast to dendrites observed in classical metal electroplating processes. These structures are in fact best described as "***moss***-like" Li as opposed to *dendritic*. This distinction is of course fundamental because it means that whereas dendritic deposition of a metal can be prevented by a variety of process and design variables (*e.g.*, by maintaining the current density below certain well-defined, fundamentally meaningful limits; by adding a supporting electrolyte salt with a cation that is electrochemically inactive at the potentials at which metal plating or stripping occurs; by using such large salt concentrations that the double layer thickness in the electrolyte is comparable to the thickness of the cation depletion zone at the diffusion limit, *etc.*), no such general or

Received: January 16, 2023
Accepted: March 31, 2023

https://doi.org/10.1021/acsenergylett.3c00120
ACS Energy Lett. 2023, 8, 2113–2121

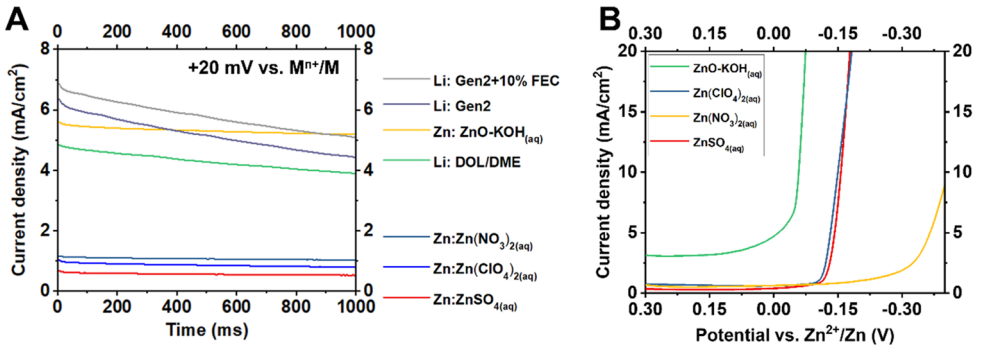

Figure 1. Electrochemical evaluation of the Faradaic reactions occurring in dissimilar electrolytes. (A) Chronoamperometry measurements of Li and Zn in various liquid electrolyte systems, respectively. The potential is held at +20 mV versus the experimental redox potential (M^{n+}/M) of the metal electrode immersed in the same electrolyte. Note that this experimental reference potential could be different from the theoretical redox potential of M^{n+}/M due to electrolyte-specific solvation/coordination effects. For example, the effective plating/stripping redox Zn in the alkaline electrolyte, i.e., $Zn(OH)_4^{2-}/Zn$, has a potential of −1.19 V, which is lower than the potential of the Zn^{2+}/Zn redox (−0.76 V) in a standard electrolyte; both are referenced against standard hydrogen electrode. (B) Linear sweep voltammetry measurements of typical Zn electrolyte systems. Scan rate: 20 mV/s. The experiments are performed in M||SS two-electrode coin cells, where M is either Zn or Li metal, and SS is a stainless-steel working electrode.

fundamentally-based strategies exist for ameliorating moss-like metal electrodeposition.

In the context of next-generation batteries using Li or Na metal anodes, the benefits of understanding mossy deposition are well-known and discussed at length in a rising number of incisive literature reviews.[8,9] Briefly, the moss-like growth is now known to be detrimental to battery operation for a number of reasons: it causes fast capacity fading, propensity for internal battery short-circuits, it facilitiates parasitic reactions that consume electrolyte components , and so on. The research of Li metal anodes over the past 10 years has revealed a number of materials design strategies that overcome these limitations in one way or another and have resulted in steady improvements in the plating/stripping reversibility of Li anodes from impractical low values to reliably above 90%; notwithstand in this progress, achieving the remaining 10% or so in reversibility, in battery cell and electrolyte designs that do not compromise the beneficial aspects of Li, is difficult but essential for progress toward all practical post-Li ion batteries.[10] Understanding and eliminating the moss-like Li growth is obviously critical to accomplishing this goal.[11] Fundamentally-based strategies for ameloriating mossy electrodeposition of metals could also offer insights into the fundamental governing principles of crystal growth in reactive environments. The inability to understand and predict the shape of crystals grown under specified conditions represents a major gap in knowledge. We note further that the moss-like growth pattern observed during electroreduction of metals has also been reported in materials synthesis using totally different methods, e.g., vapor deposition using an inert gas as the transport agent.[12] Understanding the origin of moss-like growth is therefore of interest to a broader community that is concerned with crystal growth by deposition.

The large volume of prior literature focused on improving Li metal anodes provides a good foundation for investigating the origins of mossy metal electrodeposition. Failure to stop the process—despite the range of methods proposed—attests to the robustness of the underlying mechanisms and may even mean that the moss-like growth regime is actually the preferred growth mode under typical conditions.[7] A second set of insights comes from the fact that a mossy deposition regime exists for all other alkali metals like Na and K and in essentially all electrolytes. In contrast, mossy electrodeposits are normally not observed for nonalkali metals, *e.g.*, Al, Mg, Zn, Cu, *etc.*, electrodeposited in neutral electrolytes. The moss-like growth then evidently originates from a differentiating property of the alkali metal systems.

There are at least three types of hypotheses advanced in the literature to explain why alkali metals form dominantly nonplanar electrodeposits: (a) those based on surface diffusivity, (b) those based on the cation transport rate in the electrolyte bulk, and (c) those based on chemical instability/reactivity of the metal and electrolyte.[9] For hypothesis (c), it is thought that the chemical degradation of electrolyte components (solvent, salts, additives) produces a passivating material phase (interphase) on the metal surface, known as the *solid-electrolyte interphase*, SEI. The spontaneously formed SEI is typically heterogeneous and exhibits complex chemical and morphological features. The mechanism by which the SEI causes porous growth has been under active investigation.[13] One view is that spatial heterogeneity in the SEI chemistry and thickness creates an uneven ion transport landscape at the electrode surface. Deposition therefore occurs preferentially in randomly located regions with more facile ion transport and therefore mimics the SEI heterogeneity. It has also been proposed that the reduction in surface tension by surface passivation of the metal by the SEI contributes to the propensity for aggressive growth normal to the electrode plane.[14] None of the underlying issues are fully settled, which has led to a proliferation of the literature approaching the issue of moss-like growth from different angles, *e.g.*, using a substrate that has optimal Li surface diffusivity,[15,16] choosing an electrolyte that forms a more uniform interphase on Li,[17] and employing a three-dimensional host to reduce the current density,[7] respectively. While these strategies are capable of improving the overall battery performance, their influence on the microstructure of the Li electrodeposits remains unresolved.[7]

A complementary question is whether ***non***-alkali metals that usually do not form moss-like deposits, e.g., Zn, can be driven into a moss-like regime similar to what is observed for alkali metals. We show later that identifying the special set of conditions that allow any metal to transition to moss-like growth offers critical insights about both the origin of the

https://doi.org/10.1021/acsenergylett.3c00120
ACS Energy Lett. 2023, 8, 2113−2121

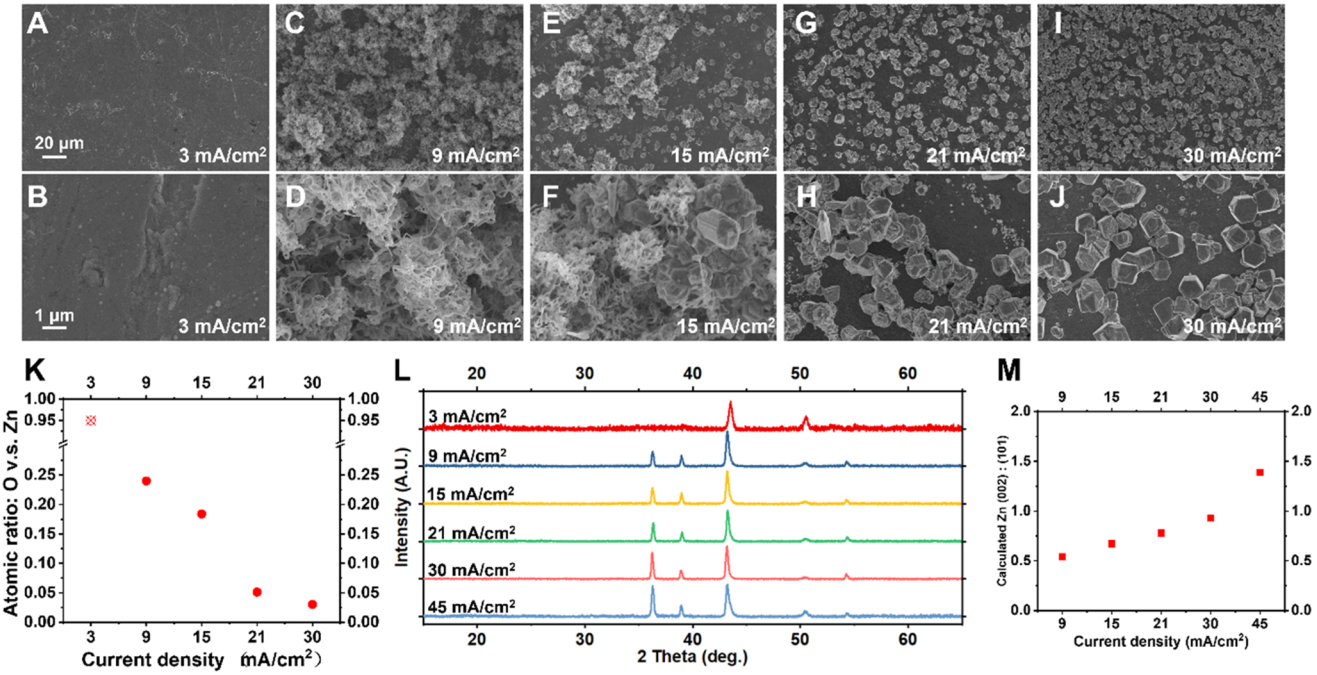

Figure 2. Microstructural and chemical characterization of Zn electrodeposits grown in a strongly alkaline electrolyte (30 wt % KOH saturated with ZnO). (A)−(J) Zn electrodeposition morphology obtained at different current densities, as specified at the lower right corner of the images. See more SEM images of the moss-like Zn electrodeposits in Figure S4. (K) EDS analysis of Zn and O of the electrodeposits. (L) XRD patterns of the electrodeposits. (M) Estimated ratio between $(002)_{Zn}$ intensity and $(101)_{Zn}$ intensity of the electrodeposits. The diffraction generated by stainless steel at around $2\theta \approx 43.5°$ was subtracted when estimating the $(002)_{Zn}$:$(101)_{Zn}$ ratio; see Figure S8. The experiments are performed in Zn||SS two-electrode coin cells; the deposition occurs on the SS electrode.

moss-like growth of alkali metals and how it might be eliminated. Zn also stands out as a good system for in-depth studies complementary to those performed in alkali metals for a number of reasons: as already noted, Zn does not form mossy deposits in mild-pH aqueous electrolytes; Zn deposition in strongly alkaline aqueous electrolytes is known to be challenged by interphase formation and large interfacial impedances; as a hexagonal crystalline material, Zn has distinctive crystallographic growth characteristics in comparison to alkali metals, which form cubic crystal lattices; finally Zn deposition can be carried out in aqueous media where inorganic compounds are the dominant and typically only interphase components formed by electroreduction of electrolyte components, this contrasts with the more complex organic−inorganic hybrid interphases formed on alkali metal anodes in aprotic organic electrolytes.

The analyses above suggest that experimental efforts focused on a 2D phase plane—with deposition rate and electrolyte chemistry being the two dimensions—could provide a fruitful approach for identifying the dominant mossy growth regime(s) in any metal. The deposition rate is easily controllable by setting the magnitude of the applied current. We first focus on the effect of electrolyte chemistry. The propensity of a given electrolyte chemistry for undergoing parasitic reactions can be evaluated using analytical electrochemical characterization tools. Figure 1A reports the current response of typical Li and Zn electrolytes in chronoamperometric measurements. The potential of the working electrode is held at +20 mV versus the experimental redox potential of the metal (Li^+/Li or Zn^{2+}/Zn). The presence of an overpotential is one requirement for metal electrodeposition to occur, which corresponds to a negative potential on the working electrode when referenced against the redox potential of the metal in question. At this slightly positive potential of +20 mV, there is no driving force for metal electrodeposition; the measured current should instead be attributable to parasitic side reactions. The magnitude of the observed response current therefore serves as both a qualitative and a quantitative indicator of the propensity of an electrolyte for decomposition at electrochemical potentials near the redox potential of the metal. It is also noticeable that the response currents observed on Li electrodes decay faster over time. This suggests that the electrolyte decomposition and interphase formation process on Li is more self-limiting than on Zn. Such a nature could be ascribed to the presence of polymeric species in the interphase on Li that acts as a "matrix" and creates a more compact film,[18] whereas the interphase on Zn is expected to be completely inorganic due to the absence of organic species in the electrolyte.

A rather large response current > 5 mA/cm² is observed for all three Li metal systems studied. The response current densities are in fact comparable to typical current densities used in contemporary studies of galvanostatic Li electrodeposition, i.e., <2 mA/cm². Under these galvanostatic conditions, the measured voltages of Li cells reportedly remain above 0 V versus Li^+/Li at the initial stage.[19] The observation of the significant response current at +20 mV versus Li^+/Li provides a straightforward explanation for the above-zero voltage capacity. It also evinces the strong propensity of the electrolytes to undergo parasitic reactions and to continuously form SEI at voltages close to the onset potential of Li electrodeposition.

We next consider the behaviors of various Zn electrolytes at slightly positive potentials (relative to Zn^{2+}/Zn). The alkaline Zn electrolyte[20] composed of 30 wt % KOH saturated by ZnO shows a response current density comparable in magnitude to

https://doi.org/10.1021/acsenergylett.3c00120
ACS Energy Lett. 2023, 8, 2113−2121

those observed for Li but nearly 1 order of magnitude higher than what are observed for the mild-pH aqueous electrolytes studied. The large current density observed in the alkaline electrolyte is attributable to parasitic reactions. This same alkaline electrolyte has been widely used in Zn battery studies. Of particular interest is that—similar to the Li electrolytes—the parasitic reactions are believed to generate solid products (e.g., ZnO)[21,22] that precipitate onto and cover the electrode surface. Based on the high impedance of a ZnO interphase, we speculate that Zn electrodeposits from the alkaline electrolytes may have a higher probability than other Zn electrolytes to develop a moss-like morphology, analogous to the Li systems. And the alkaline Zn electrolyte offers a unique, powerful platform for interrogating the role played by chemical instability and SEI formation in the electrodeposition of Zn.

To further investigate the Faradaic processes occurring in the regime close to the onset of Zn plating/stripping, we performed linear sweep voltammetry (LSV) measurements in the Zn electrolytes (Figure 1B). These measurements are performed in two-electrode coin cells, but see also Figure S1 for LSV data collected using a three-electrode setup; based on the comparison between results from two-electrode and three-electrode setups, no significant deviation is introduced in this specific study by shorting the reference electrode and the counter electrode in a two-electrode coin-cell setup. Consistent with the chronoamperometric tests, the alkaline Zn electrolyte exhibits the highest parasitic reaction current in the positive potential range (i.e., from +0.30 to 0 V versus Zn^{2+}/Zn). Another significant finding is that the faradaic current above 0 V versus Zn^{2+}/Zn originating from the parasitic reactions is not as sensitive to the overpotential. The weaker dependence of rates of parasitic reactions upon the overpotential could reflect the fact that metal deposition has a higher exchange current density than the electrolyte decomposition reactions. It in fact remains around 3 mA/cm^2 over the full positive potential range. This insensitivity contrasts starkly with the nearly exponential current−voltage relationship observed after the onset potential (slightly negative) for Zn electroreduction is reached. We believe that this difference is central to understanding the competing nature of the faradaic reactions in electrodeposition and how this competition influences the electrodeposit growth morphology. The ratio between the deposition current and the parasitic reactions current can be manipulated by imposing different overpotentials in a potentiostatic electrodeposition or current densities in a galvanostatic deposition. For example, at a smaller overpotential/current, the parasitic reactions are more prominent, resulting in a faster rate of SEI formation relative to metal deposition. The balance is reversed at high overpotentials/currents.

On this basis, one would expect that moss-like growth is most likely at low current/overpotential regimes and can be arrested in the high current/overpotential regimes. We note that this expectation is exactly opposite to the conclusion one would reach using any of the transport-based hypotheses. Figure 2A−J reports the morphologies of Zn electrodeposits obtained in the alkaline electrolytes at different current densities (i.e., 3, 9, 15, 21, 30 mA/cm^2, respectively). As evidenced by these SEM images, the growth pattern of Zn is sensitive to the current density. At 3 mA/cm^2, the potential is above 0 V versus Zn^{2+}/Zn (Figure S2), meaning that the Faradaic current observed should not be attributed to Zn deposition. Instead, parasitic reactions contribute the majority—if not the whole—of the measured current. In particular, no reversible plating/stripping behavior is detected in the Coulombic efficiency measurement under the low current density condition (Figure S3). This is also confirmed in the SEM characterization—no Zn deposit is observable. Instead, a number of oxygen-enriched small particles are detected. EDS analysis shows the O:Zn atomic ratio is close to 1:1. This suggests that ZnO is the dominant interphase species, which is consistent with prior literature.[21,22] This means that either no Zn is formed or the Zn deposits are so porous/loose that they detach easily from the substrates during the deposition process. Taken together, these results demonstrate that—surprisingly—the galvanostatic electrochemical response of Zn in alkaline aqueous electrolytes at low current densities is dominated by chemical instability.

Interestingly, the Zn deposits show a characteristic moss-like morphology at a higher current density 9 mA/cm^2; see high-magnification images in Figure S4. As the current density increases, the Zn morphology transitions gradually to a more well-defined crystalline morphology composed of particulate crystallites. The shapes of the particles follow those deduced from the theoretically predicted Wulff construction for the hexagonal close packed Zn crystal. Specifically, at 15 mA/cm^2, the growth pattern is a mixture of the moss-like deposits and the crystalline deposits; see also optical microscopy and 2D height profiling in Figures S5−S6. Whereas at 30 mA/cm^2, the crystalline particles dominate! This morphological evolution of Zn over the applied current density is in good agreement with earlier studies.[23,24] In tandem with the transition to compact Zn electrodeposits, the O:Zn ratio continues to decrease from 0.24:1 at 9 mA/cm^2 to 0.03:1 at 30 mA/cm^2 (Figure 2K). These results support the conclusion that the SEI has a more pronounced effect at lower currents than at higher currents (i.e., content and effect of SEI: 9 mA/cm^2 > 15 mA/cm^2 > 21 mA/cm^2 > 30 mA/cm^2).

The morphological transition seen in Figures 2A-2J is also reflected in part by the crystallographic features of the electrodeposits. Consistent with the microstructure characterization, at 3 mA/cm^2, only the X-ray diffraction (XRD) peak of the stainless-steel substrate is detectable, suggesting parasitic reactions dominate the Faradaic response under this condition. Starting from 9 mA/cm^2, characteristic diffraction peaks corresponding to $(002)_{Zn}$, $(100)_{Zn}$, and $(101)_{Zn}$ are detected. A key finding is that the $(002)_{Zn}$ diffraction intensifies as the current density increases. This point can be clearly seen from the plot in Figure 2M, which shows the ratio between $(002)_{Zn}$ and $(101)_{Zn}$; see also Figure S7. This ratio serves as a rough qualitative estimate of the out-of-plane orientational order of the deposits. The randomness associated with crystallographic texture of the deposits formed at low current densities is a manifestation of the random orientation and alignment of the individual Zn wires in the moss-like electrodeposits. The intensification of the $(002)_{Zn}$ at a relatively higher current density is consistent with what is reported in less SEI-forming electrolytes, e.g., $ZnSO_{4(aq)}$, where Zn crystallites tend to align the basal (002) plane horizontally with respect to the electrode surface.[25] These results about the Zn morphology developed in the alkaline electrolyte should be compared to the surface morphology formed in other Zn electrolytes that exhibit smaller Faradaic contributions from parasitic reactions (Figure 1 and Figure S8).

Next, we used a rotating disk electrode (RDE) to resolve the chemical and the transport aspects involved in the deposition

https://doi.org/10.1021/acsenergylett.3c00120
ACS Energy Lett. 2023, 8, 2113−2121

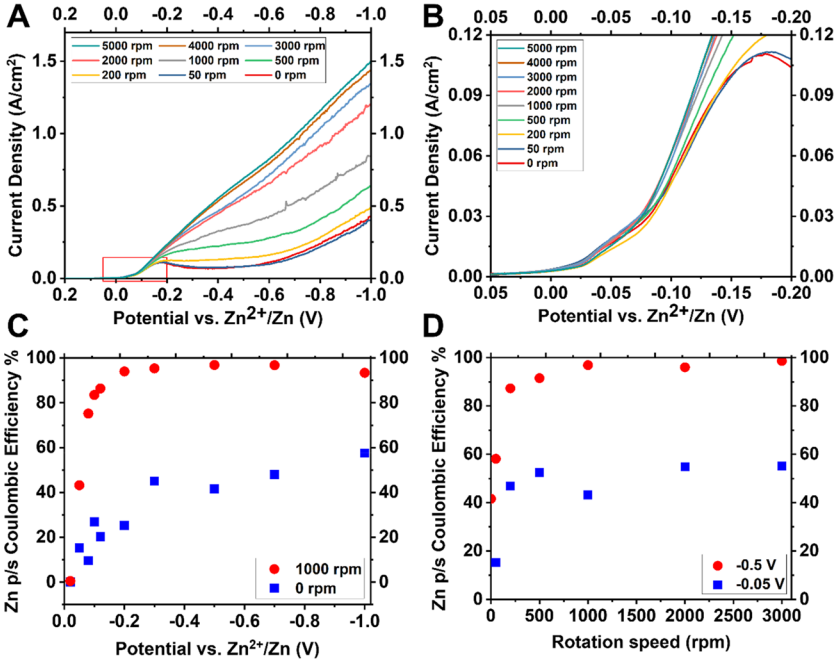

Figure 3. Zn plating/stripping in the strongly alkaline electrolyte (30 wt % KOH saturated with ZnO) at a rotating disk electrode. (A) Linear sweep voltammetry measurements under different electrode rotation speeds. (B) Magnified plot showing the $i-V$ plot near the onset of Zn plating. Dependence of Zn plating/stripping Coulombic efficiency (C) on the potential at fixed rotation speeds and (D) on the rotation speed at fixed overpotentials. (D). Experiments were performed in a commercial (Pine Research) three-electrode rotating disk cell. Both the reference electrode and the counter electrode are made of Zn; stainless steel is used as the working electrode.

process (Figure 3). The rationale for using an RDE is manifold. The RDE facilitates detailed electrochemical analysis in a three-electrode configuration, which enables more precise conclusions than what are possible from the two-electrode systems, e.g., coin cells. Additionally, electrochemical measurements in an RDE allow the mass transport near the electrode to be precisely controlled by imposing a well-defined convective flow by rotating the working electrode. Analysis of the momentum balance equations for a Newtonian liquid electrolyte yields an approximate, but closed-form expression (the Levich equation: $\delta = \frac{D_0^{1/3}\nu^{1/6}}{0.620\omega^{1/2}}$), for the thickness of the hydrodynamic boundary layer.[26,27] Here, D_0 is the diffusivity, ν is the kinematic viscosity of the solution, and ω is the angular rotation speed. Figures 3A and 3B summarize the main LSV measurements for Zn in alkaline electrolytes. At rotation speeds ranging from 0 to 5000 rpm, the system exhibits a typical $i-V$ response to the negative potential sweep. As shown in the magnified plot in Figure 3B, the response starts with a regime controlled by electrochemical kinetics, captured by the Butler–Volmer equation, before entering the diffusion-limited regime with a limiting current density around 100 mA/cm^2. Of particular note is that the $i-V$ relation in the initial regime shows negligible dependence on the rotation speed. It means that mass transport does not play an important role in the electrochemical process within this range (i.e., <100 mA/cm^2). We examined the Zn electrodeposit morphology on the working electrode of the RDE (Figure S9). The results are evidently consistent with those obtained from the coin-cell experiments reported in Figure 2. These observations show that the morphological transitions of Zn electrodeposits at low current densities (e.g., in Figure 2) cannot be attributed to mass transport related origins.

It is believed that the plating/stripping reversibility of metal electrodeposits is fundamentally correlated to their morphology. Motivated by this hypothesis, we measured the plating/stripping Coulombic efficiency of the Zn electrodeposits formed under different overpotential and rotation conditions (Figures 3C and 3D). At low overpotentials where Zn forms moss-like deposits, the plating/stripping Coulombic efficiency is consistently low (i.e., <90%), regardless of the rotation conditions. As the overpotential increases, the system however quickly enters the diffusion limited regime, which results in a porous, chemotactic growth pattern and incomplete stripping.[25] In this regime, rotation-induced convective flow provides effective enhancement in mass transport and remarkably improves the plating/stripping efficiency. These findings based on Zn metal (Figures 1–3) reveal the two types of instabilities of fundamentally different origins, as illustrated in Scheme 1: the excessive SEI formation due to parasitic reactions at the low current/overpotential regime and the diffusion limit at the high current/overpotential regime, respectively. Stable electrodeposition is achievable at moderately high currents/overpotentials away from both instabilities or at high currents/overpotentials with enhanced mass transport—for example—enabled by artificial convective flow.

We next apply the insights gained from studying Zn to understand the origin of moss-like Li growth. The current densities used for Li deposition in contemporary literature is <5 mA/cm^2, sometimes <1 mA/cm^2. Comparing these values to current densities associated with the parasitic reactions reported in Figure 1A, it is reasonable to conclude that the parasitic reactions that form heterogeneous SEI play a key role in the formation of moss-like Li within the low current/overpotential regime. Approaches for circumventing the moss-like Li growth can therefore be devised by leveraging these understandings. Figure 4A reports the LSV investigation of Li

https://doi.org/10.1021/acsenergylett.3c00120
ACS Energy Lett. 2023, 8, 2113–2121

Scheme 1. Illustration Showing the Two Instabilities That Drive the Porous Growth of Metals in Battery Anodes[a]

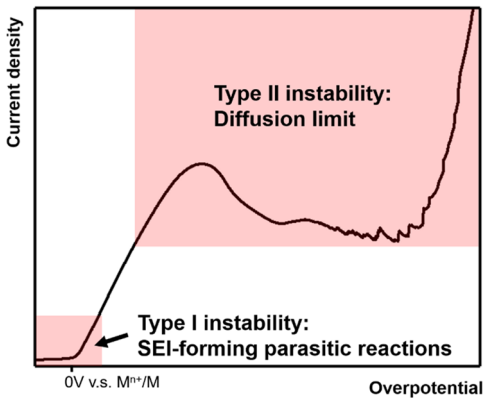

[a]Type I and Type II instabilities manifest themselves as moss-like and dendrite-like growth modes, respectively.

deposition from a carbonate-based electrolyte at different rotation speeds. Analogous to the Zn deposition from the alkaline electrolyte, the $i-V$ response of this Li electrolyte transitions from a first regime (at low currents/overpotentials) where it is relatively insensitive to rotation speed. This is followed by a second regime at larger currents/overpotentials where the $i-V$ response is highly sensitive to the rotation speed. Based on the understandings gained from the Zn case, we hypothesize that simultaneously applying a large overpotential and imposing a rotation-induced convective flow would provide a mechanism for obtaining smooth-planar Li deposits in any electrolyte. Figure 4B summarizes the Li electrodeposit morphology obtained at a large overpotential of −2 V versus Li^+/Li at different rotation speeds; see also Figure S10 for larger images. Without rotation, the Li metal undergoes an outward, chemotaxis-type growth due to mass transport limit as previously reported.[25] As the rotation speed increases, this outward growth is gradually suppressed and completely eliminated at rotation speeds greater than 1000 rpm. Surprisingly, under this condition, the Li metal forms a uniform deposition layer composed of sphere-shape particles! This is in stark contrast to the moss-like morphology reported consistently in prior literature[7] (see also Figure S11). The successful elimination of the moss-like growth pattern of Li using the method of high potential plus rotation further supports that both of the instabilities illustrated in Scheme 1 must be simultaneously suppressed in order to promote uniform, compact deposition morphology desirable in rechargeable battery anodes. As an empirical rule, the applied current density i should be within this range to avoid both instabilities: $10\ i_s < i < 0.8\ i_{lim}$, where i_s is the side reaction rate that can be estimated based on measurements performed in Figure 1, and i_{lim} is the limiting current density determined by the mass transport properties of the electrolyte. This provides key implications for electrolyte design; it suggests that an ideal electrolyte has a small i_s and a large i_{lim}, creating a broad stable regime in between for the applied current density. It is particularly important for large-scale cells as the current distribution is not necessarily uniform across an electrode, meaning that the effective i_{eff} could deviate from the nominal

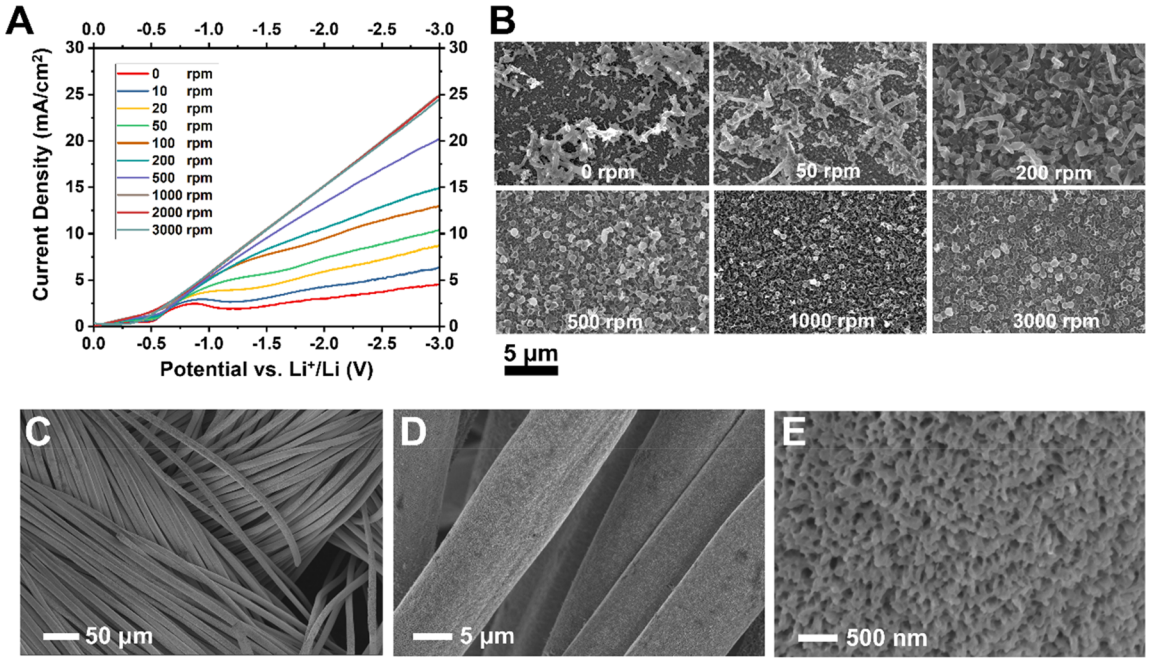

Figure 4. Understanding the electrochemical growth patterns of Li electrodes. (A) Linear sweep voltammetry measurements of Li plating on a rotating disc electrode made of glassy carbon, at different rotation speeds. Electrolyte: 50 mM $LiPF_6$ in EC/DMC with 10% FEC. (B) SEM images of Li metal deposition morphology at −2.0 V versus Li^+/Li at a rotating disc electrode at different rotation speeds. The experiments were performed in a three-electrode rotating disk apparatus. Two pieces of Li foils are used as the reference electrode and the counter electrode, respectively; glassy carbon is used as the working electrode. (C)(D)(E) Electrodeposition morphology of Li on a nonplanar substrate at −1.6 V versus Li^+/Li (areal capacity: 0.5 mAh/cm^2; current density: ~10^2 mA/cm^2) in a stagnant electrolyte at different magnifications. Electrolyte: 1 M $LiPF_6$ in EC/DMC with 10% FEC. The experiments reported in (C), (D), and (E) are performed in Li‖CC two-electrode coin cells; the deposition occurs on the CC electrode. The current density is calculated based on the macroscopic area of the electrode.

https://doi.org/10.1021/acsenergylett.3c00120
ACS Energy Lett. 2023, 8, 2113−2121

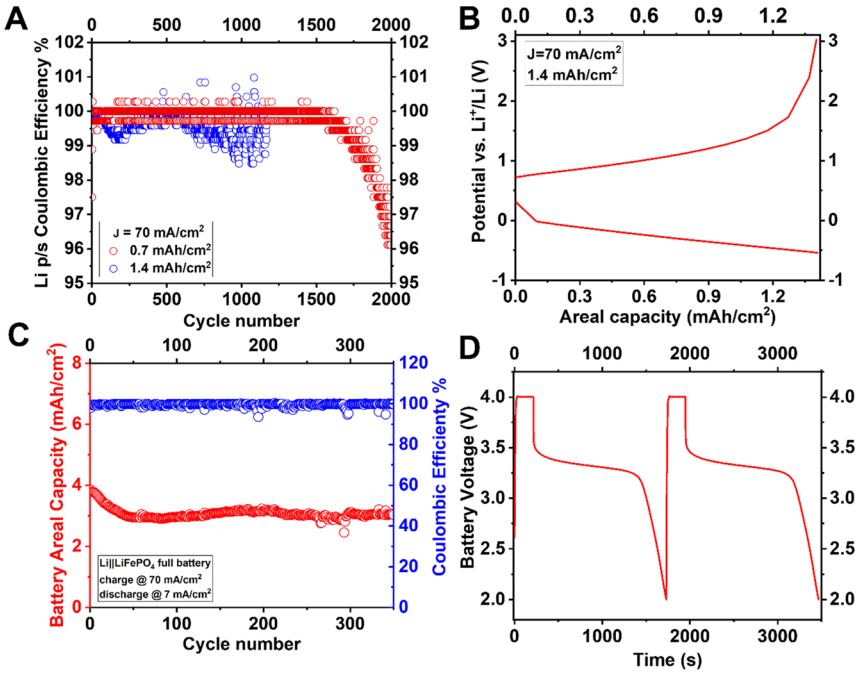

Figure 5. Electrochemical reversibility of Li metal anodes at high rates. (A) Li plating/stripping Coulombic efficiency in a 1 M LiTFSI DOL/DME electrolyte obtained at 70 mA/cm^2 and (B) the corresponding voltage profile. Li||CC two-electrode coin cells are used for these experiments; the deposition/dissolution occurs on the CC electrode. (C) Li||$LiFePO_4$ full battery cycling performance using a charging current density of ∼70 mA/cm^2 and (D) the voltage profiles of the 100th and 101st cycles. The cell is charged to and then held at 4 V until the current density drops from 70 mA/cm^2 to 30 mA/cm^2. Electrolyte: 1 M $LiPF_6$ in EC/DMC with 10% FEC. A carbon-fiber cloth is used as an anode current collector in all these cells. The experiments were performed using two-electrode prelithiated CC (10 mAh/cm^2)||LFP coin cells.

applied current i. A broader stable regime therefore guarantees that i_{eff} falls into such a regime when subjected to practical cycling. We further point out that the morphological evolution in the dissolution of metals[28] could also be strongly dependent on the applied current density[29] and imposes a nontrivial impact on the overall reversibility of the deposition-dissolution reactions in battery anodes.

While the effectiveness of the combined high potential and rotation is self-evident from the results in Figure 4B, it is understood that introducing such flows in more common battery configurations—e.g., closed cells—would pose a potentially unsurmountable challenge. Alternative approaches exist for enhancing mass transport, which are compatible with constraints imposed by a closed battery cell. Specifically, it has been reported in previous studies that nonplanar electrode architectures may serve to reduce the local current density and thereby increase the effective mass transport at an electrode. Our previous work[7] also shows that, at a low current densities, nonplanar substrates (e.g., interwoven carbon fibers) have negligible influence on the deposition morphology—the Li metal consistently grows into the moss-like structures and does not form a conformal deposition layer on the individual carbon fibers. Figure 4C−E shows the analogous results when Li is deposited on interwoven carbon fibers from 1 M $LiPF_6$ in the carbonate-based electrolyte. The deposition is performed at a large overpotential of −1.6 V versus Li^+/Li. The Li forms a highly conformal deposition layer covering the surface of the individual carbon fibers. Figure S12 shows a similar Li deposition morphology in an ether-based electrolyte. The consistency suggests this is a generalizable approach for eliminating the moss-like growth mode of Li. This morphology should be compared to Li deposition on carbon fibers at a lower current (see ref 7). This result, again, corroborates our finding that the moss-like growth pattern is due to the competing parasitic Faradaic reactions at low currents/potentials and can be suppressed via rational designs of the electrokinetics. We further test the relevance of these discoveries to developing high-performance Li metal batteries. Stable Li plating/stripping behaviors over thousands of cycles are observed at a high current density of 70 mA/cm^2 (Figures 5A-5B). The larger variation and shorter cycle life of the cell with a higher areal capacity are expected. At high current densities, the concentration gradient near the electrode develops over prolonged deposition and incurs interfacial instability.[25] A full-cell test using the $LiFePO_4$ cathode illustrates a capacity retention of 80% over 350 cycles, with a high charging current density of 70 mA/cm^2 and a normal discharging current density of 7 mA/cm^2 (Figures 5C-5D). Full cells using a planar Li electrode, by contrast, claim minimal effective capacity due to sluggish kinetics (Figure S13). It should be noted that the Coulombic efficiency measured in full cells with prelithiated anodes does not directly evaluate the metal plating/stripping reversibility, in contrast to the measurements in Figures 5A-5B. The close-to-unity Coulombic efficiency values in Figure 5C suggest that irreversible parasitic reactions do not contribute nontrivially to the capacity measured in the charging process and that there are no microshorts that lead to ineffective charging and self-discharge.

The results reported in the present study offer critical insights into the origin of moss-like electrodeposit growth during recharge of metal battery anodes. The first two of the three hypotheses normally used to explain nonplanar metal deposition, i.e., the surface diffusivity and the electrolyte cation

https://doi.org/10.1021/acsenergylett.3c00120
ACS Energy Lett. 2023, 8, 2113−2121

diffusivity hypotheses—have been examined using a combination of a rotating disk electrode and electrodeposition at variable overpotentials. Our results show that neither are important in the regime where mossy deposition of metals is observed. Specifically, a smooth, compact metal electrodeposit morphology is expected at a low current density, where the surface diffusion and the electrolyte cation diffusion are relatively fast, and kinetical instabilities are suppressed. On the other hand, porous deposition morphology (e.g., moss-like) should emerge at a high current density, where these two types of diffusion are slow relative to the deposition rate, and kinetical instabilities are therefore activated. The key findings from this study reported in Figures 2-4 contradict these expectations.

Our results are consistent with a third hypothesis—the chemical instability of the electrolyte. Specifically, upon electrodeposition, two competing reactions, i.e., the reduction of the metal cations and the parasitic reduction of electrolyte components, occur simultaneously on the electrode surface. The solid products of these parasitic reactions, e.g., polymers, inorganic compounds, *etc*., passivate the electrode surface nonuniformly, promoting "hot spots" in the growth landscape where the passivation layer is thinner and/or of a chemistry that facilitates deposition. As such, in considering the hypothesis, an additional degree of freedom is involved: electrolyte chemistry. The rate of the parasitic reaction is directly dependent on the chemistry of the liquid electrolyte in contact with the electrode surface and is therefore highly tunable by varying the electrolyte composition. This is consistent with our experimental observations that moss-like growth is predominant in electrolytes associated with a lower chemical stability and at small current densities where the rate of SEI-forming parasitic reactions is comparable to or higher than the rate of metal electrodeposition. The moss-like growth of metals in electroplating is therefore attributable to the competing Faradaic reactions—i.e., the SEI-forming parasitic reactions and the metal electrodeposition reaction—occurring on the electrode surface.

In conclusion, comparing the electrokinetics-morphology relations manifested in the electrodeposition of Zn and Li in a group of representative electrolytes, respectively, we demonstrate unambiguously that the moss-like growth electrodeposit predominates in strongly-SEI forming electrolytes, particularly in the low-current density regime. In this regime, the competition is between the Faradaic reactions—i.e., SEI formation and metal deposition. A thick SEI gives rise to the moss-like growth because of nonuniform transport landscape, reduction in surface tension, or both at the same time.[14,30] Surprisingly, the persistent moss-like growth mode is readily suppressed at higher current densities, where the rate at which metal is deposited substantially exceeds—i.e., is roughly 1 order of magnitude higher than the rate at which SEI-forming parasitic reactions occur. Consistent with results from proof-of-concept full cell battery tests reported, knowledge from the study uncovers—counterintuitively—the promise held by fast charged battery electrodes.

■ ASSOCIATED CONTENT

Data Availability Statement

All data needed to evaluate the conclusions in the paper are present in the paper and/or the Supporting Information.

Supporting Information

The Supporting Information is available free of charge at https://pubs.acs.org/doi/10.1021/acsenergylett.3c00120.

Materials and Methods, potential profiles, surface topography, SEM images (PDF)

■ AUTHOR INFORMATION

Corresponding Author

Lynden A. Archer − *Department of Materials Science and Engineering and Robert Frederick Smith School of Chemical and Biomolecular Engineering, Cornell University, Ithaca, New York 14853, United States;* orcid.org/0000-0001-9032-2772; Email: laa25@cornell.edu

Authors

J. X. Kent Zheng − *Department of Materials Science and Engineering, Cornell University, Ithaca, New York 14853, United States; Department of Physics, Massachusetts Institute of Technology, Cambridge, Massachusetts 02139, United States*

Jiefu Yin − *Robert Frederick Smith School of Chemical and Biomolecular Engineering, Cornell University, Ithaca, New York 14853, United States*

Tian Tang − *Department of Materials Science and Engineering, Cornell University, Ithaca, New York 14853, United States*

Complete contact information is available at: https://pubs.acs.org/10.1021/acsenergylett.3c00120

Author Contributions

L.A.A. directed the project. J.X.K.Z. and L.A.A. conceived and designed this work. J.X.K.Z., J.Y., and T.T. performed the electrodeposition, electrochemical measurements, and structure characterizations. All the authors analyzed and discussed the data. J.X.K.Z. and L.A.A. wrote the manuscript with important input from all the authors.

Funding

This work was supported by DOE BES under award # DE-SC0016082 and as part of the Center for Mesoscale Transport Properties, an Energy Frontier Research Center supported by the U.S. Department of Energy, Office of Science, Basic Energy Sciences, under award #DE-SC0012673. This work made use of the Cornell Center for Materials Research Shared Facilities which are supported through the NSF MRSEC program (DMR-1719875).

Notes

The authors declare no competing financial interest.

■ ACKNOWLEDGMENTS

J.X.K.Z. expresses his gratitude to Prof. J. G. Checkelsky for support and discussions.

■ REFERENCES

(1) Lee, B.; Paek, E.; Mitlin, D.; Lee, S. W. Sodium metal anodes: emerging solutions to dendrite growth. *Chem. Rev.* **2019**, *119* (8), 5416−5460.

(2) Zheng, J.; Archer, L. A. Controlling electrochemical growth of metallic zinc electrodes: Toward affordable rechargeable energy storage systems. *Science Advances* **2021**, *7* (2), No. eabe0219.

(3) Kurz, W.; Fisher, D. J. Dendrite growth in eutectic alloys: the coupled zone. *International Metals Reviews* **1979**, *24* (1), 177−204.

(4) Shimada, W.; Furukawa, Y. Pattern formation of ice crystals during free growth in supercooled water. *J. Phys. Chem. B* **1997**, *101* (32), 6171−6173.
(5) Kim, J. T.; Jorné, J. The Kinetics and Mass Transfer of Zinc Electrode in Acidic Zinc-Chloride Solution. *J. Electrochem. Soc.* **1980**, *127* (1), 8.
(6) Yang, Y.; Zeng, H.; Wang, D.; Wu, Y.; Chen, J.; Huang, Y.; Wang, P.; Feng, W. Fractal Growth of Quasi Two-Dimensional Copper Dendrites by Template-free Electrodeposition. *Langmuir* **2023**, *39* (8), 3045−3051.
(7) Zheng, J.; Tang, T.; Zhao, Q.; Liu, X.; Deng, Y.; Archer, L. A. Physical orphaning versus chemical instability: is dendritic electrodeposition of Li fatal? *ACS Energy Letters* **2019**, *4* (6), 1349−1355.
(8) Chen, X. R.; Zhao, B. C.; Yan, C.; Zhang, Q. Review on Li deposition in working batteries: from nucleation to early growth. *Adv. Mater.* **2021**, *33* (8), 2004128.
(9) Zheng, J.; Kim, M. S.; Tu, Z.; Choudhury, S.; Tang, T.; Archer, L. A. Regulating electrodeposition morphology of lithium: towards commercially relevant secondary Li metal batteries. *Chem. Soc. Rev.* **2020**, *49* (9), 2701−2750.
(10) Zheng, J. X. K. Perspective—Reversibility of Electro-Plating/Stripping Reactions: Metal Anodes for Rechargeable Batteries. *J. Electrochem. Soc.* **2022**, *169* (10), 100532.
(11) Lin, D.; Liu, Y.; Li, Y.; Li, Y.; Pei, A.; Xie, J.; Huang, W.; Cui, Y. Fast galvanic lithium corrosion involving a Kirkendall-type mechanism. *Nature Chem.* **2019**, *11* (4), 382.
(12) Chen, Y. J.; Chi, B.; Zhang, H. Z.; Chen, H.; Chen, Y. Controlled growth of zinc nanowires. *Mater. Lett.* **2007**, *61* (1), 144−147.
(13) Mistry, A.; Fear, C.; Carter, R.; Love, C. T.; Mukherjee, P. P. Electrolyte confinement alters lithium electrodeposition. *ACS Energy Letters* **2019**, *4* (1), 156−162.
(14) Hagopian, A.; Doublet, M.-L.; Filhol, J.-S. Thermodynamic origin of dendrite growth in metal anode batteries. *Energy Environ. Sci.* **2020**, *13* (12), 5186−5197.
(15) Wang, J.; Zhang, J.; Duan, S.; Jia, L.; Xiao, Q.; Liu, H.; Hu, H.; Cheng, S.; Zhang, Z.; Li, L.; Duan, W.; Zhang, Y.; Lin, H. Lithium Atom Surface Diffusion and Delocalized Deposition Propelled by Atomic Metal Catalyst toward Ultrahigh-Capacity Dendrite-Free Lithium Anode. *Nano Lett.* **2022**, *22* (19), 8008−8017.
(16) Røe, I. T.; Schnell, S. K. Slow surface diffusion on Cu substrates in Li metal batteries. *Journal of Materials Chemistry A* **2021**, *9* (17), 11042−11048.
(17) Biswal, P.; Kludze, A.; Rodrigues, J.; Deng, Y.; Moon, T.; Stalin, S.; Zhao, Q.; Yin, J.; Kourkoutis, L. F.; Archer, L. A. The early-stage growth and reversibility of Li electrodeposition in Br-rich electrolytes. *Proc. Natl. Acad. Sci. U. S. A.* **2021**, *118* (2), No. e2012071118.
(18) Li, Y.; Li, Y.; Pei, A.; Yan, K.; Sun, Y.; Wu, C.-L.; Joubert, L.-M.; Chin, R.; Koh, A. L.; Yu, Y.; et al. Atomic structure of sensitive battery materials and interfaces revealed by cryo−electron microscopy. *Science* **2017**, *358* (6362), 506−510.
(19) Biswal, P.; Stalin, S.; Kludze, A.; Choudhury, S.; Archer, L. A. Nucleation and Early Stage Growth of Li Electrodeposits. *Nano Lett.* **2019**, *19* (11), 8191−8200.
(20) Lim, M. B.; Lambert, T. N.; Ruiz, E. I. Effect of ZnO-saturated electrolyte on rechargeable alkaline zinc batteries at increased depth-of-discharge. *J. Electrochem. Soc.* **2020**, *167* (6), 060508.
(21) Pourzolfaghar, H.; Hosseini, S.; Zuki, F. M.; Alinejad, M.; Li, Y.-Y. Recent advancements to mitigate zinc oxide formation in zinc-air batteries: A technical review. *Materials Today Communications* **2021**, *29*, 102954.
(22) Wang, J.-G.; Tian, M.-L.; Kumar, N.; Mallouk, T. E. Controllable template synthesis of superconducting Zn nanowires with different microstructures by electrochemical deposition. *Nano Lett.* **2005**, *5* (7), 1247−1253.
(23) Otani, T.; Nagata, M.; Fukunaka, Y.; Homma, T. Morphological evolution of mossy structures during the electrodeposition of zinc from an alkaline zincate solution. *Electrochim. Acta* **2016**, *206*, 366−373.
(24) Ito, Y.; Wei, X.; Desai, D.; Steingart, D.; Banerjee, S. An indicator of zinc morphology transition in flowing alkaline electrolyte. *J. Power Sources* **2012**, *211*, 119−128.
(25) Zheng, J.; Yin, J.; Zhang, D.; Li, G.; Bock, D. C.; Tang, T.; Zhao, Q.; Liu, X.; Warren, A.; Deng, Y. Spontaneous and field-induced crystallographic reorientation of metal electrodeposits at battery anodes. *Science Advances* **2020**, *6* (25), No. eabb1122.
(26) Buck, R. P.; Keller, H. E. Chronopotentiometry at Rotating Disk Electrodes. *Anal. Chem.* **1963**, *35* (3), 400−402.
(27) Koutetskii, Y. A.; Levich, V. G. e. The use of a rotating disc electrode for studying kinetic and catalytic processes in electrochemistry. *Dokl. Akad. Nauk SSSR* **1957**, *117*, 441−444.
(28) Sanchez, A. J.; Kazyak, E.; Chen, Y.; Lasso, J.; Dasgupta, N. P. Lithium stripping: anisotropic evolution and faceting of pits revealed by operando 3-D microscopy. *Journal of Materials Chemistry A* **2021**, *9* (37), 21013−21023.
(29) Laycock, N. J.; Newman, R. C. Localised dissolution kinetics, salt films and pitting potentials. *Corrosion science* **1997**, *39* (10−11), 1771−1790.
(30) Tikekar, M. D.; Choudhury, S.; Tu, Z.; Archer, L. A. Design principles for electrolytes and interfaces for stable lithium-metal batteries. *Nature Energy* **2016**, *1* (9), 16114.

https://doi.org/10.1021/acsenergylett.3c00120
ACS Energy Lett. 2023, 8, 2113−2121